# Martensite formation in Ti–Al layers produced by laser surface alloying

J. H. Abboud and D. R. F. West

*The microstructures of Ti–Al layers produced by laser surface alloying of a Ti substrate have been investigated for Al contents in the range 17–36 at.-%. The alloyed layers were obtained using a continuous wave $CO_2$ laser and a powder feed technique employing the following laser processing parameters: 1·8 kW power, 3 mm beam diameter, 7 mm $s^{-1}$ traverse speed, and feedrates of Al powder ranging from 0·03 to 0·07 g $s^{-1}$. The microstructures were disordered lath martensite α′ in 17 at.-% Al alloy, ordered massive and acicular martensite in 23 at.-% Al alloy, and ordered massive, acicular, and lath martensite in 30 and 36 at.-% Al alloys. The change in martensite type and morphology is discussed in relation to the available data for the β to α′ transformation in Ti alloys.*

*MST/1437*

 *Manuscript received 4 March 1991; in final form 5 April 1991.* *The authors are in the Department of Materials, Imperial College of Science, Technology and Medicine, London.*

## Introduction

In recent years, there has been a considerable amount of work on rapid solidification processing of Ti alloys. This includes melt spinning,[1,2] atomisation,[3] and laser surface melting.[4,5] The objectives of these methods include refinement of the microstructures, reducing the scale of segregation, and obtaining supersaturated solid solutions. Comprehensive reviews of the work can be found in Refs. 6–8.

For Ti–Al alloys (particularly when the Al content exceeds 10 at.-%) there has been relatively little work. For example, Jackson *et al.*[9] have made a comparison between the microstructures of $Ti_3Al$–1Zr produced by ingot metallurgy and by melt spinning. They found that rapid solidification processing results in significant refinement of the microstructure. In both methods, the microstructures were identified as hcp, characteristic of $\alpha_2$; ordering was not prevented by the rapid cooling and the size of the antiphase boundaries was 10–20 nm compared with 600–1200 nm in the conventionally processed alloy.

Although laser surface melting and solidification can be used effectively to produce high cooling rates typically up to $10^5$ K $s^{-1}$, there have been few applications of this procedure to Ti–Al alloys. Some observations have been recently reported by the authors[10] on the use of a continuous wave (CW) $CO_2$ laser and powder feed technique to produce rapidly solidified Ti–Al alloyed layers. The composition and the volume of the alloyed zone can be controlled by selection of appropriate laser processing parameters. Some microstructural observations on Ti–Al alloyed layers containing 30 and 50 at.-%Al have also been briefly reported.[11]

In the present paper, a detailed study of the microstructures of some laser surface Ti–Al alloyed layers in the composition range 17–36 at.-%Al is reported.

## Experimental procedure

Laser surface melting of a commercial purity Ti plate of 10 mm thickness was carried out using a 2 kW CW $CO_2$ laser (Control Laser Ltd). Commercial purity Al powder (100 μm average particle size) was blown into the melt zone of the Ti using a stream of argon gas. During the process, a very effective shrouding system was used involving a central jet and an outer general flow of argon. Analysis of two of the alloyed regions showed an oxygen content of ~0·23 wt-% compared with a value of less than ~0·13 wt-% for the substrate. In considering the possibility of using the alloying procedure as a means of producing oxidation resistant surface layers, this level of contamination by oxygen may be acceptable.

A laser beam of 3 mm diameter at 1·8 kW power was used and the feedrate of Al powder was varied to produce Ti–Al alloyed layers containing different amounts of Al. The relative speed between the substrate and the laser beam was kept constant at 7 mm $s^{-1}$. (The laser processing parameters have been established by prior experimentation.[10])

The alloyed layers were sectioned transversely and prepared for metallography by grinding (from 120 to 1200 grit), polishing with alumina (from 5 to 0·05 μm), and etching with a solution of 2%HF, 10%$HNO_3$, 88% distilled water. Scanning electron microscopy (SEM) linked with an energy dispersive spectrometer (EDS) was used for structural and compositional analysis. Thin foils were prepared for transmission (TEM) and scanning transmission electron microscopy (STEM) by cutting a thin (~1 mm) slice parallel to the surface of the laser alloyed zone. The slices were mechanically ground to ~100 μm and discs of 3 mm diameter were obtained using a spark erosion machine. Electropolishing was carried out using a twin jet apparatus employing a solution containing 10% sulphuric acid in methanol at 18 V and at a temperature of −30°C. The thin foils examined were estimated to be located at approximately the mid-depth position of the alloyed zones.

## Results

### ALLOY LAYER COMPOSITIONS

The average compositions of the Ti–Al alloyed layers produced by varying the feedrate are given in Table 1. Several areas (5 × 5 μm) of each individual alloyed zone

**Table 1 Average Al contents of Ti–Al alloyed layers produced using laser operating conditions of 1·8 kW, 3 mm beam diameter, and 7 mm $s^{-1}$ traverse speed**

| Powder feedrate, g $s^{-1}$ | Al, at.-% |
|---|---|
| 0·033 | 17 |
| 0·055 | 23 |
| 0·060 | 30 |
| 0·066 | 36 |

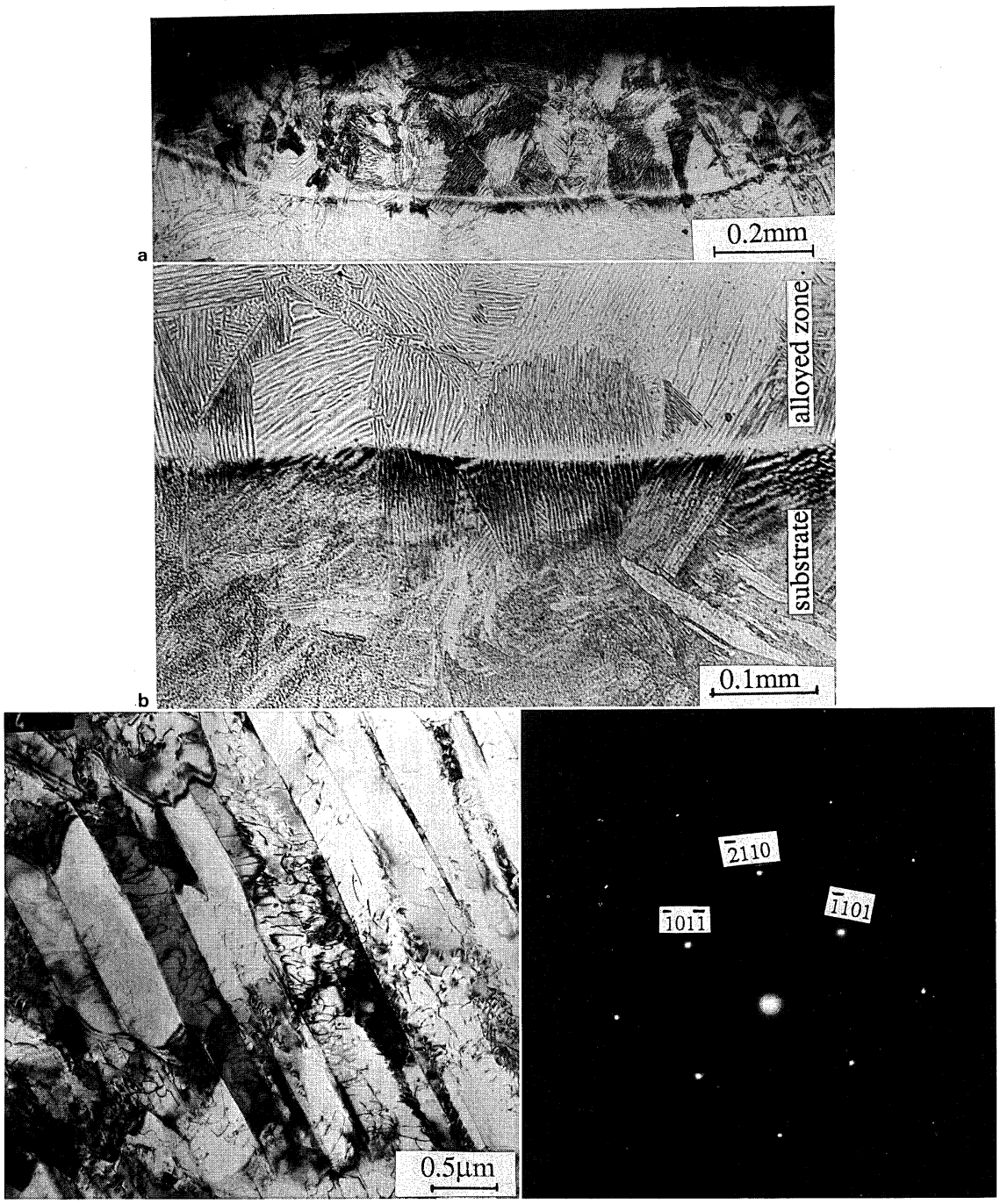


*a* optical macrograph; *b* optical micrograph showing epitaxial growth from substrate; *c* bright field TEM; *d* selected area diffraction pattern (SADP), zone axis $[0\bar{1}11]_\alpha$

**1 Ti–17 at.-%Al laser alloyed layer**

were examined using EDS X-ray analysis and relatively uniform composition and scatter within about ±1 at.-%Al were revealed.

## MICROSTRUCTURES

### Ti–17 at.-%Al

A transverse section of the laser alloyed zone is shown in Fig. 1*a*. Large columnar grains of width 0·1 mm, showing a martensitic structure, have grown epitaxially from the $\beta$ grains in the substrate towards the surface (Fig. 1*b*). A martensitic structure was observed within the grains. The heat affected zone, within which the temperature reached the $\beta$ range, with subsequent rapid cooling, consisted of coarse lath martensite, which contained a high density of dislocations. The width of the martensite laths ranged between 1 and 10 μm. The martensite in the laser surface alloyed zone was also coarse and consisted of parallel sided laths; some lath thickness values of ~1 μm were also observed (Fig. 1*c*). Selected area diffraction patterns (SADPs) taken from this martensite were indexed as hcp crystal structure (Fig. 1*d*). Retained $\beta$ was not detected, which indicates complete transformation of $\beta$ to martensite during cooling. Also, superlattice reflections were not observed showing that this martensite was disordered ($\alpha'$).

### Ti–23 at.-%Al

The structure of this alloyed layer is shown in Fig. 2*a*. Grains of $\beta$, 0·1–0·2 mm in width, originated epitaxially from the substrate and grew during solidification towards the surface. Two types of microstructural feature were

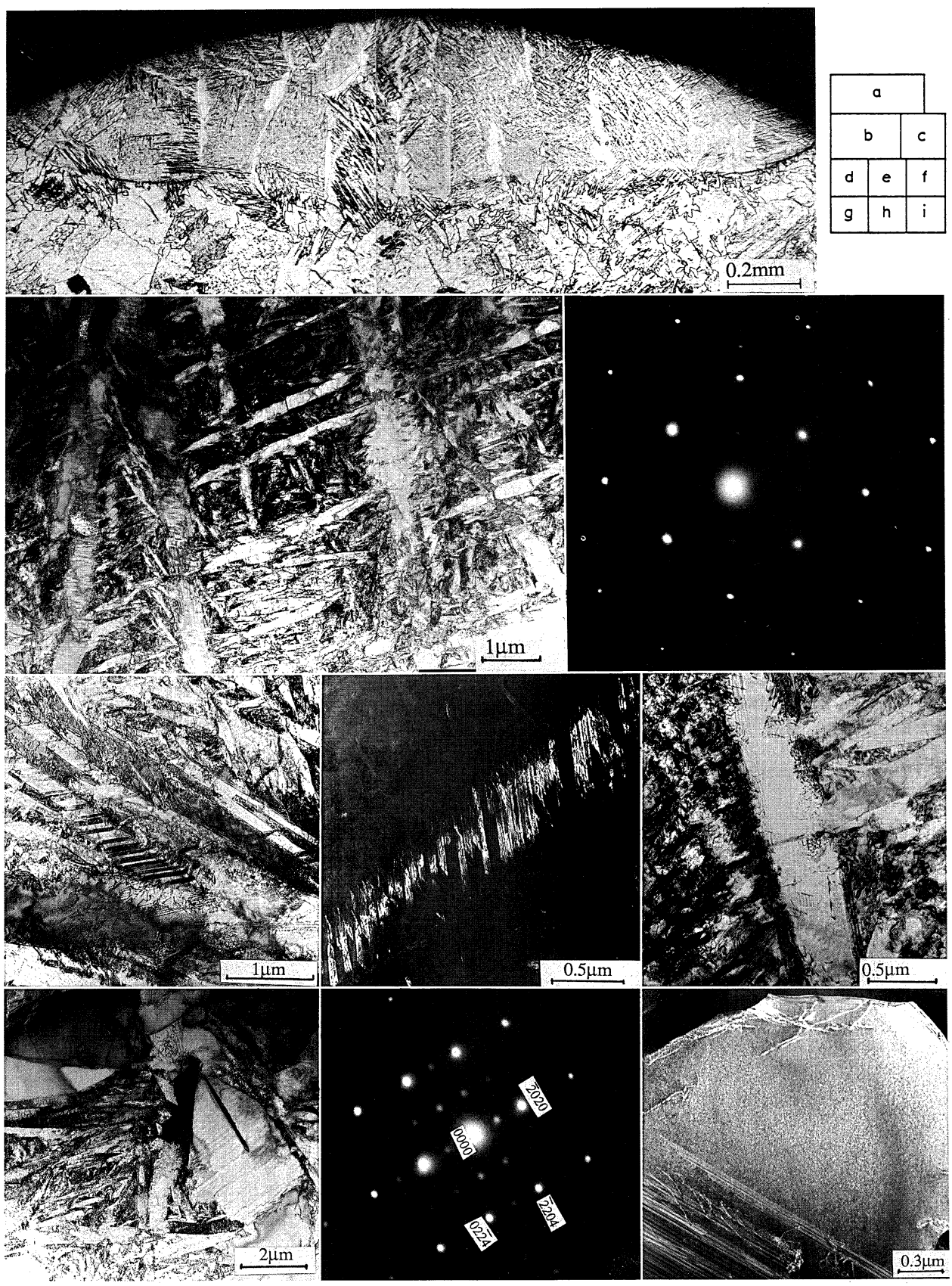


*a* optical macrograph; *b* bright field TEM showing martensite in alloyed zone; *c* SADP (indexing as in Fig. 1*d*), zone axis $[01\bar{1}1]_{\alpha'_2}$; *d* bright field TEM showing twinned plate; *e* dark field TEM using $(1\bar{1}01)_{\alpha'_2}$; *f* bright field TEM showing secondary plate nucleated from primary plate; *g* TEM showing massive and acicular martensite; *h* SADP taken from massive martensite, zone axis is $[24\bar{2}\bar{3}]_{\alpha'_2}$; *i* dark field TEM using $(10\bar{1}0)_{\alpha'_2}$ reflection showing fine antiphase boundaries

## 2 Ti–23 at.-%Al laser alloyed layer

observed: irregularly shaped regions located at the original $\beta$ grain boundaries, typical of massive transformation products, and termed massive martensite[12] and fine plate martensite, in the grains, which was in contact with, and originated from, the massive martensite. Compositional analysis using the EDS X-ray technique did not show any difference in composition between the massive martensite and the fine plate martensite. Also, SEM using back scattered electrons did not reveal any contrast between the two types of microstructure. Optical microscopy of the plate martensite at relatively high magnification revealed a linear feature running down the centre of the plate over its entire length. This feature has been observed previously in $\alpha$ Ti martensite and in other types and is termed a midrib.[13]

The observations made using TEM are presented in Figs. 2*b*–2*k*. The martensite was acicular, consisting of primary plates of width 0·25–0·5 μm and smaller secondary plates of size <0·1 μm; some of the secondary plates originated from the primary plates. A discontinuity along the primary plates and the presence of lines in the middle of the plate resembled a midrib appearance; some of the plates contained a relatively low density of dislocations. Selected area diffraction patterns taken from the plates were indexed as hcp crystal structure and showed the presence of faint superlattice reflections (Fig. 2*c*). Efforts to use these superlattice reflections to detect antiphase boundaries were unsuccessful owing to either short range order or the presence of antiphase boundaries of size below the resolution of the technique, i.e. ~2·5 nm. Substructural features, such as twinning in the martensite plates were observed (Fig. 2*d*); a SADP taken from the twinned plate was indexed and the twin plane was $(1\bar{1}01)$, which is very common in Ti martensite.

The massive martensite appeared in TEM as large grains (Fig. 2*g*); some of the grains showed stacking faults, whereas others showed a featureless structure (apart from a small number of dislocations). Selected area diffraction patterns from the massive martensite were indexed as hcp crystal structure with superlattice reflections more intense than those from the plates (Fig. 2*h*). Dark field imaging using a $(10\bar{1}0)$ superlattice reflection revealed very fine antiphase boundaries, of size 20–25 nm, within the grains (Fig. 2*i*). Using data from SADPs taken from the massive martensite and from martensite plates, and on the basis of the presence of antiphase boundaries, it is considered that the microstructure of this alloy consisted of ordered massive martensite $\alpha_2^m$ and ordered plate martensite $\alpha'_2$.

### Ti–30 at.-%Al

The structure of this laser alloyed layer was similar to that of the Ti–23 at.-%Al layer (Fig. 3*a*). The width of the original $\beta$ grains was 0·1–0·2 mm and the growth was epitaxial from the substrate. Observations using TEM showed acicular martensite characterised by primary plates of ~100 μm length and 0·25 μm width and secondary plates of ~0·5 μm length and <0·1 μm width (Fig. 3*b*). Most of the plates were internally slipped; twinned plates were not observed. A small amount of lath martensite was observed coexisting with massive martensite (Fig. 3*c*). Selected area diffraction patterns taken from the plates were indexed as hcp crystal structure with superlattice reflections more intense than in the Ti–23 at.-%Al alloy. Dark field imaging using a superlattice reflection showed the presence of fine (~25 nm) antiphase boundaries within the primary and secondary plates; no preferential alignment of the domains was observed (Fig. 3*d*). The massive martensite appeared in TEM as a featureless structure apart from a few dislocations. Selected area diffraction patterns from the massive martensite were indexed as hcp crystal structure with superlattice reflections. Dark field images showed antiphase boundaries of size ~30 to 50 nm (Fig. 3*e*), which were a little larger than in the Ti–23 at.-%Al alloy (~25 nm). From TEM, it was shown that the massive martensite and the fine martensite plates were ordered and the microstructure is considered to be $\alpha_2^m + \alpha'_2$.

### Ti–36 at.-%Al

The structure of this laser alloyed layer was similar to that of Ti–30 at.-%Al, but with a greater proportion of massive martensite $\alpha_2^m$ (Fig. 4*a*). Three distinct types of microstructure were observed: massive martensite $\alpha_2^m$, coarse lath martensite, and acicular martensite. The proportions of lath and massive martensite were higher than those observed in the Ti–23 at.-%Al and Ti–30 at.-%Al alloyed layers. Using TEM, the presence of acicular and coarse lath martensite and featureless areas was observed (Figs. 4*b* and 4*c*). Selected area diffraction patterns from these structures were indexed as ordered hcp crystal structure (Fig. 4*d*). Antiphase boundaries were observed (Fig. 4*e*), which were larger (50–70 nm) than those observed in the Ti–30 at.-%Al alloy. The domains did not show any preferential alignment. Using SEM and STEM on the bulk sample and the thin foil did not reveal any difference in composition between the various microstructural features. $\gamma$ phase (TiAl) was not detected in this alloy either by TEM examination or by X-ray diffraction analysis.

## Discussion

### MARTENSITIC TRANSFORMATION

Following solidification to form $\beta$ phase[14,15] the cooling rate in the solid state was sufficiently rapid to produce martensite in all the alloys. The variation of martensite type and morphology (i.e. massive, lath, and acicular) as a function of Al content (Table 2) is not fully understood in the context of previous work on martensite formation in Ti alloys. However, it is of interest to consider the changes in relation to the available data on the variation of $M_s$ temperature with Al content in the Ti–Al system.

### $M_s$ TEMPERATURE

Jepson *et al.*[17] reported a progressive increase in $M_s$ temperature with increasing Al content up to 20 at.-%Al, but there appears to be no experimental data for higher Al contents. The $M_s$ versus composition curve was approximately 10–20 K below the $\alpha/\alpha+\beta$ boundary of the phase diagram and their results were consistent with the calculated $T_0$ data, lying ~40 K below the $T_0$ data.

**Table 2 Approximate estimate of proportions of types of martensite in laser surface Ti–Al alloyed layers**

| Al, at.-% | Type of martensite |
|---|---|
| 17 | Lath |
| 23 | 10% massive + acicular |
| 30 | 10% massive + acicular + small proportion of lath |
| 36 | 20% massive + acicular + 25% lath |

Lath refers to the type of martensite which appears in the form of colonies of parallel sided laths separated by a high density of dislocations; each lath in the colony has the same variant of the orientation relationship. Massive martensite refers to the featureless regions positioned adjacent to the prior $\beta$ grain boundaries, coexisting with conventional martensite in alloys containing 23, 30, and 36 at.-%Al. In the literature (e.g. Ref. 16), the term massive martensite has sometimes been applied to the lath morphology product. Acicular martensite refers to plates showing different variants of orientation; these plates were frequently internally twinned.

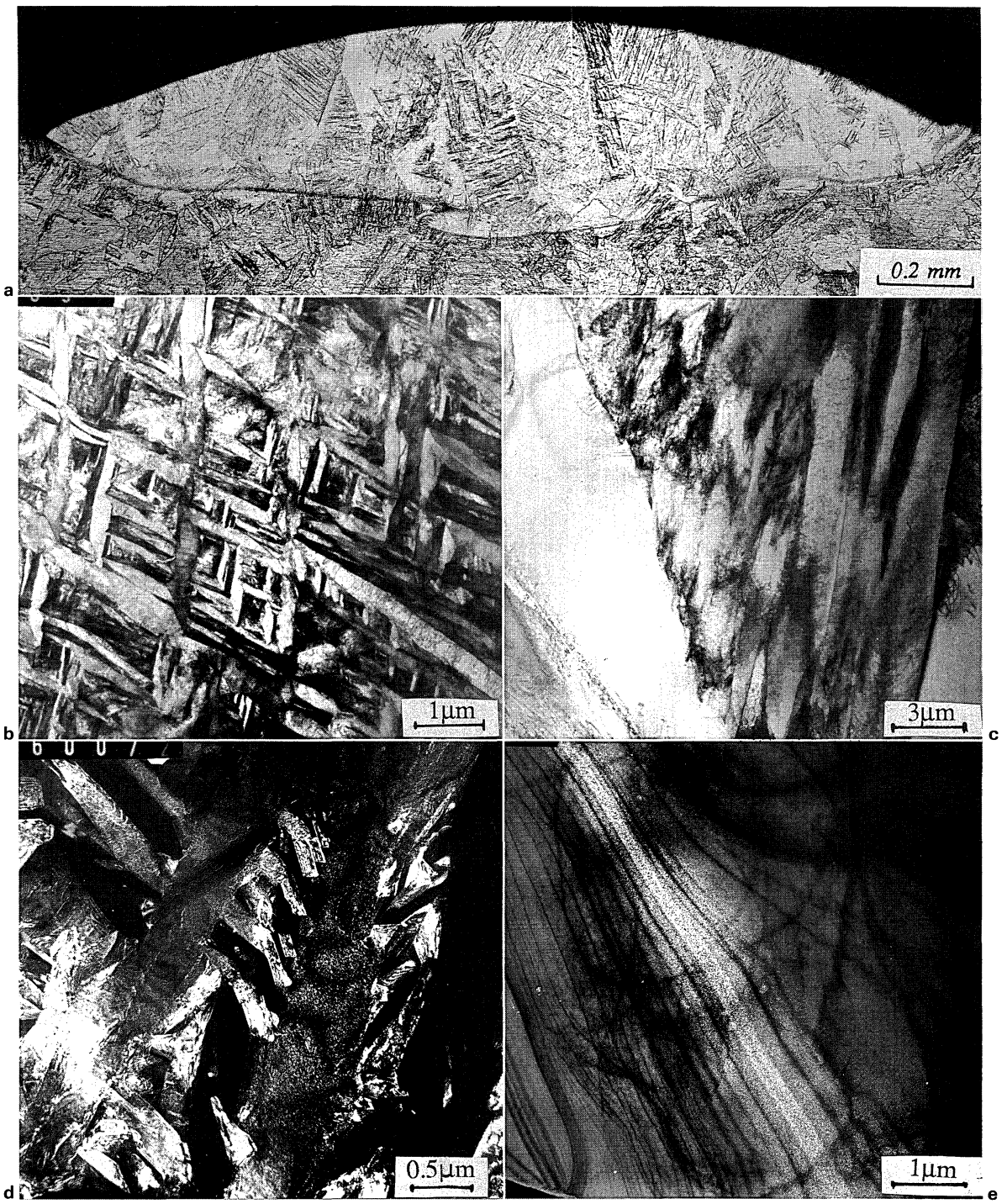


*a* optical macrograph; *b* TEM showing acicular martensite; *c* TEM showing massive and lath martensite; *d* dark field TEM showing antiphase boundaries in plate martensite; *e* dark field TEM showing antiphase boundaries in massive martensite

**3 Ti–30 at.-%Al laser alloyed layer**

The experimental $M_s$ values of Sato *et al.*[18] were significantly lower than those of Jepson *et al.*:[17] for compositions between ~1 and 13 at.-%Al, their values lay in the approximate range 810–830°C compared with ~930°C reported by Jepson *et al.* at 10 at.-%Al. The reasons for this difference are not clear, since results from the two investigations[17,18] for Ti–Nb alloys are in reasonable agreement. It is possible that oxygen, although an $\alpha$ stabiliser, may lower the $M_s$ temperature through its solid solution strengthening effect as discussed below for other elements.

The cooling rates in the laser alloyed samples in the temperature range of martensite formation are[10] of the order of 500–1000 K $s^{-1}$. The $M_s$ values studied in the present work are for comparable cooling rates. Although Jepson *et al.* used low oxygen content Ti for alloy preparation, the oxygen contents of the samples after use in experiments to determine the $M_s$ were not reported. The oxygen levels in the present work may be somewhat higher than those in the work of Jepson *et al.*

## MASSIVE MARTENSITE

The transformation to massive martensite, which is interpreted as producing the 'featureless' regions occurring at grain boundaries in the alloys containing 23–36 at.-%Al (Table 2) has been studied extensively in Fe based and Cu based alloy systems.[19–20] It is defined as a diffusionless

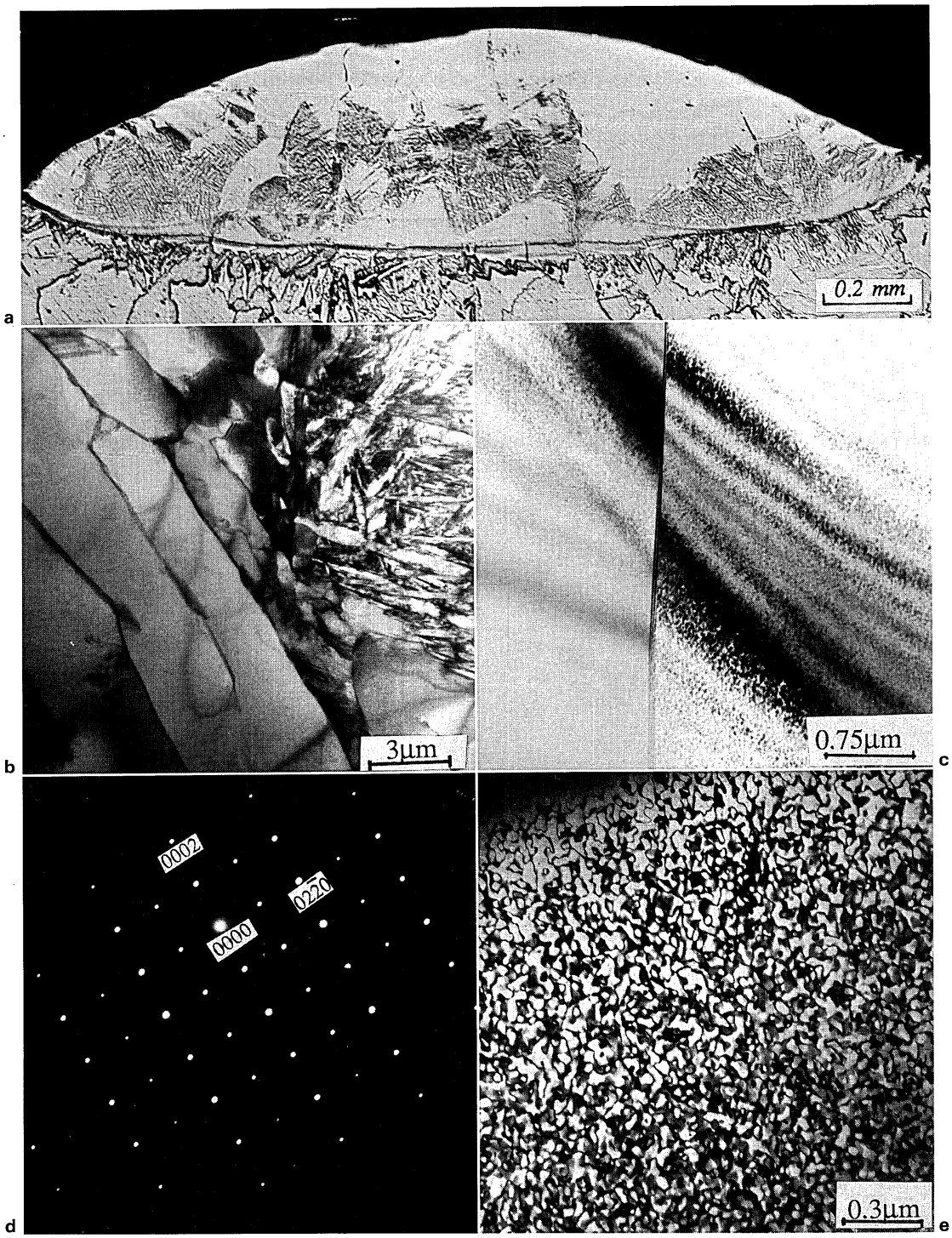


*a* optical macrograph; *b*, *c* TEMs; *d* SADP taken from massive martensite, zone axis $[2\bar{1}\bar{1}0]_{\alpha_2^m}$; *e* dark field TEM showing antiphase boundaries

**4 Ti–36 at.-%Al laser alloyed layer**

'civilian' transformation with interface migration involving thermal activation and it can be represented as a C curve on a time–temperature–transformation (TTT) diagram.[21] A start temperature $M_a$ can be located between $T_0$ and $M_s$. Higher cooling rates, above a critical value, can prevent the transformation to massive martensite leading to conventional martensite formation. Among the characteristic features of the massive martensite are its preferential formation at grain boundaries, irregular interfaces with the matrix, and the absence of compositional differences between the matrix and the massive product; these features were observed in the present work. Plitcha *et al.*[12] have investigated the transformation to massive martensite in the Ti eutectoid systems, e.g. Ti–Ag, Ti–Au, and Ti–Si. They reported that three basic requirements must be satisfied to allow this type of transformation to occur. First, the $T_0$ temperature must be high enough to allow atomic jumps across the interface to take place at a reasonable rate. Second, the kinetics of any competing precipitation reactions must be relatively slow. In this context, it was deduced that a narrow interval between the transus and the $T_0$ temperature, i.e. a narrow nearly horizontal two phase region in the phase diagram, is favourable to transformation to massive martensite. This is because the value of the driving force for the equilibrium transformation at $T_0$ is then relatively small. Third, the

product phase must have a reasonably wide range of existence to favour this type of transformation. Taking account of these points, predictions[12] as to possible systems in which the transformation to massive martensite could occur included the Ti–Al system. The present results demonstrate the validity of this prediction.

The observed increase in the proportion of massive martensite with increasing Al content (Table 2) can be correlated with the increase in $M_s$ temperature which could lead to higher critical cooling rates being required to suppress martensite; it may also be noted that the volume of the alloyed zones increased with increasing Al content, thus causing some reduction in cooling rates and a greater tendency to form massive martensite.

### LATH–ACICULAR TRANSITION

The transition from lath to acicular martensite with increasing solute content in $\beta$ stabilised Ti alloy systems such as Ti–Mo has been the subject of a number of studies (e.g. Ref. 16). Also, the comparable transition in Fe based alloys has been extensively investigated (e.g. Ref. 20). In both of these groups of alloys, the $M_s$ temperature is substantially depressed by solute additions. Among the factors considered to cause the lath–acicular transition is the increase in flow stress of the matrix phase associated with increased solid solution hardening which necessitates an increased driving force to propagate the matrix/martensite interface. Davis *et al.*[16] have suggested that lath martensite formation occurs when slip takes place in the $\beta$ phase ahead of the $\alpha'$ crystals to reduce the shape strain and when solid solution strengthening of the $\beta$ phase occurs to such an extent that slip is prevented, acicular martensite forms.

In the present work, there was a transition from coarse lath to acicular martensite between 17 and 23 at.-%Al: at higher Al contents the proportion of acicular martensite decreased slightly by replacement with some lath martensite. These changes, occurring over a range of increasing $M_s$, are unexpected. It is of interest to note that the morphology variation between 17 and 23 at.-%Al alloys was accompanied by a change from disordered to ordered martensite. However, it is not apparent how the morphology change could be dependent on the ordering reaction, since an ordering process cannot occur concurrently with the shear type transformation. Instead, disordered martensite forms initially followed by ordering. It is suggested that the morphology change observed in the present work may be qualitatively interpreted in relation to two opposing solid solution strengthening effects of Al. First, at a given temperature, the stength of the $\beta$ increases in proportion to $\sqrt{C}$, where $C$ is the atomic concentration of Al. Second, as the $M_s$ temperature increases, the strength of the $\beta$ at the $M_s$ tends to decrease by the normal temperature dependence effect. It is possible that between 17 and 23 at.-%Al, the effect of the atomic concentration of Al dominates, favouring acicular martensite, whereas at higher Al contents the temperature dependence effect is more significant, thus favouring some lath formation. It should also be noted that there may be differences in oxygen contents between the various zones studied, which might affect the morphology observed.

### ORDERING OF MARTENSITE

According to Blackburn,[22] when the Al content exceeds ~10 at.-% in the binary Ti–Al system, ordering occurs within the $\alpha$ by the formation of antiphase boundaries. He has also shown that quenching Ti–25 at.-%Al alloy from the $\beta$ field produces a martensite lath structure containing domains of size 5–10 nm. In the present work, fine antiphase boundaries were observed within the massive martensite, whereas in the plate martensite they were difficult to resolve. In the alloys containing 30 or 36 at.-%Al, the antiphase boundaries were observed to have a tendency to increase in domain size with increasing Al content. This observation is consistent with an increase in the ordering temperature with increasing Al content.

## Conclusions

Microstructural study of the laser surface alloyed Ti–Al layers showed the presence of disordered lath martensite $\alpha'$ in 17 at.-%Al alloy; ordered massive and acicular martensite in 23 at.-%Al alloy; and ordered massive, acicular, and lath martensite in 30 and 36 at.-%Al alloys. The transition from lath (17 at.-%Al alloy) to acicular (23 at.-%Al alloy) martensite was interpreted to be a result of either solid solution strengthening or differences in oxygen content. The increase in the proportion of massive martensite with increasing Al content is consistent with an increase in the $M_s$ temperature.

## Acknowledgments

Acknowledgments are made to the Ministry of Education, Iraq, for the award of a scholarship to one of the authors (JHA); to the SERC for financial support; and to IMI Titanium Ltd for supplying the titanium.

## References

1. S. M. L. SASTRY, T. C. PENG, P. J. MESCHTER, and J. E. O'NEAL: *J. Met.*, Sept. 1983, **35**, 21.
2. T. F. BRODERICK, A. G. JACKSON, H. JONES, and F. H. FROES: *Metall. Trans.*, Nov. 1985, **16A**, 1951.
3. D. G. KONITZER, K. W. WALTERS, E. L. HEISER, and H. L. FRASER: *Metall. Trans.*, March 1984, **15B**, 149.
4. L. S. CHUMBLEY, M. A. OHLES, and F. H. FRASER: in Proc. Conf. 'Titanium rapid solidification technology', (ed. F. H. Froes and D. Eylon), 211; 1986, Warrendale, PA, The Metallurgical Society of AIME.
5. D. G. KONITZER, B. C. MUDDLE, and H. L. FRASER: *Metall. Trans.*, Oct. 1983, **14A**, 1979.
6. A. G. JACKSON, D. EYLON, and S. M. L. SASTRY: in Proc. Conf. 'Titanium rapid solidification technology', (ed. F. H. Froes and D. Eylon), 365; 1986, Warrendale, PA, The Metallurgical Society of AIME.
7. S. KRISHNAMURTHY and F. H. FROES: *Int. Mater. Rev.*, 1989, **34**, (6), 297.
8. R. G. ROWE and F. H. FROES: in Proc. Conf. 'Processing of structural metals by rapid solidification', (ed. F. H. Froes and S. J. Savage); 1986, Metals Park. OH, ASM.
9. A. G. JACKSON, K. R. TEAL, F. H. FROES, and S. J. SAVAGE: in Proc. MRS Symp. 'Rapidly solidified alloys and their mechanical and magnetic properties', (ed. D. R. Polk and A. L. Taub), 58; 1986, Pittsburgh, PA, Materials Research Society.
10. J. H. ABBOUD and D. R. F. WEST: *Mater. Sci. Technol.*, 1991, **7**, (4), 353–356.
11. J. H. ABBOUD and D. R. F. WEST: *J. Mater. Sci. Lett.*, 1990, **9**, 308.
12. M. R. PLICHTA, J. C. WILLIAMS, and H. I. AARONSON: *Metall. Trans.*, 1977, **8A**, 1885.
13. H. M. FLOWER, P. R. SWANN, and D. R. F. WEST: *J. Met.*, 1972, **7**, 929.
14. J. L. MURRAY: 'Binary alloy phase diagrams', (ed. T. B. Massalski), 173; 1986, Metals Park, OH, ASM.
15. S. E. McCULLOUGH, J. J. VALENCIA, C. G. LEVI, and R. MEHRABIAN: *Acta Metall.*, 1989, **35**, (5), 1321.
16. R. DAVIS, H. M. FLOWER, and D. R. F. WEST: *J. Mater. Sci.*, 1979, **14**, 712.

17. K. S. JEPSON, A. R. G. BROWN, and J. A. GRAY: in Proc. Conf. 'The science, technology, and application of titanium', (ed. R. I. Jaffee and N. E. Promisel); 1970, TMS-AIME and ASM.
18. T. SATO, S.HUKAI, and C. HUANG: *J. Austr. Inst. Met.*, 1960, **5**, (2), 149.
19. T. B. MASSALSKI: 'Phase transformations', 435; 1968, Metals Park, OH, ASM.
20. E. KRAUSS and A. R. MARDER: *Metall. Trans.*, 1971, **2**, 2343.
21. D. A. PORTER and K. E. EASTERLING: 'Phase transformations in metals and alloys', 349–358; 1981, Wokingham, Berks, Van Nostrand Reinhold (UK).
22. M. J. BLACKBURN: *Trans. AIME*, Aug. 1976, **239**, 1200.